

Fermi level fluctuations and the role of reduced effective mass and Zeeman splitting in the Quantum oscillations in Nodal line semimetals

Anupam Saha, Satyaki Kar*

AKPC Mahavidyalaya, Bengali, West Bengal -712611, India

Quantum oscillation measurements are crucial for nodal line semimetals in determining electronic Berry phases and thus topological nature of its magnetic oscillations. Here we study a continuum model of a nodal line semimetal under strong magnetic field and report the characteristics of the Landau level spectra and the fluctuations in the Fermi level as the field in a direction perpendicular to the nodal plane is varied through. From the obtained results on magnetization, we demonstrate the growth of quantum oscillation with field strength as well as its constancy in period when plotted against $1/B$. Furthermore we find that the density of states which show series of peaks in succession, witness bifurcation of such peaks due to Zeeman contributions. For field normal to nodal plane, such bifurcations are discernible only if the electron effective mass is considerably smaller than its free value, which usually happens in these systems. Though a reduced effective mass m^* causes the Zeeman splitting to become small compared to Landau level spacings, experimental results indicate a manyfold increase in the Lande g factor which again signifies the Zeeman contribution. For field direction in the nodal plane, the density of state peaks do not repeat periodically with energy anymore. The spectra become more spread out and the Zeeman splittings less prominent and the low energy topological regime shrinks further with reduced m^* values.

I. INTRODUCTION

Nodal line semimetals¹⁻³ (NLSM) have become popular candidate among topological semimetals⁴ due to their exotic features that are rapidly getting exposed in recent times. Its easy tunability to convert into other exotic materials such as a Weyl semimetal⁵⁻⁷, Dirac semimetals^{5,6}, magnetic semiconductors⁶ etc has also made these compounds interesting to the condensed matter community. A NLSM is characterized by topologically robust nodal ring or loops where the conduction and valence bands meet. Landau quantization develops under the influence of strong magnetic fields in such systems⁸⁻¹⁰ which substantially changes the spectral features. With field perpendicular to the nodal plane one can analytically obtain the Landau quantized spectra starting from naive continuum models of such systems. However a field in the nodal plane disrupts the planar symmetry and one needs to resort to numerics to deal with such problems. Here we consider both the situations and try to estimate few important aspects including quantum oscillations that results when the magnetic field strength is varied through.

The Landau tube widths and hence the density of states (DOS) profile changes continually with magnetic field. It causes the chemical potential (μ) to experience oscillations as the field is varied through. Not only just μ , oscillations appear in many physical variables such as magnetization, conductivity as well and such responses can be seen in NLSM compounds. If Zeeman field term is considered in addition, splitting of the DOS peaks are obtained, though it can be noticed if the electronic effective mass is considerably smaller than the free electron mass as the LL spacing become much larger compared to the Zeeman splitting under such scenario.

Now such magnetic oscillations can be topological or trivial depending on the direction of the field applied and in fact nontrivial topology is obtained when the magnetic

field contain nonzero components in the nodal plane^{9,11}. In this regard, here we also address the spectral features and their connection to topology as the field direction is confined in the nodal plane. The recent theoretical studies on quantum oscillations in NLSM systems does not discuss much about Zeeman splitting in the spectra or in general the variation of effective masses (m^*) as a magnetic field is applied, even though experimentally the Zeeman splittings are well observed at low temperatures and low fields as well as low m^* values are reported. Here in this article we would like to theoretically examine that aspect of the problem and look for any interesting physics that it leads to.

The paper is organized as follows. In section II, we give the formulation for NLSM model under the influence of magnetic field perpendicular to the nodal plane. In section III, we discuss the Fermi level fluctuation and quantum oscillations in magnetization. Section IV deals with effective mass reduction, Zeeman contributions whereas section V describes the density of states. In section VI we consider the field direction to be in the nodal plane and briefly repeat the earlier steps for this scenario. Finally we summarize our work in section VII.

II. SPECTRAL FORMULATION

Let us consider a simple NLSM Hamiltonian^{12,13} given as

$$H_0 = \left(\frac{\hbar^2 k_{\perp}^2}{2m^*} - m_0 \right) \sigma_z + v \hbar k_z \sigma_y \quad (1)$$

where $k_{\perp}^2 = k_x^2 + k_y^2$ and m^* denotes the effective mass of the band electrons.

In presence of a magnetic field perpendicular to the nodal plane in a nodal line semimetal, the Zeeman term

or the coupling of spins with the field result in shift of nodal loops to nonzero energies. The Hamiltonian becomes

$$H = \left(\frac{\hbar^2 k_{\perp}^2}{2m^*} - m_0 \right) \sigma_z \tau_0 + v \hbar k'_z \sigma_y \tau_0 + b \sigma_0 \tau_z \quad (2)$$

where the last term represent the Zeeman interaction with $b = g\mu_B B/2$ and Peierls's substituted momentum $\mathbf{k}' = \mathbf{k} - \mathbf{eA}/\hbar$. The σ (τ) matrices are the Pauli matrices describing orbital (spin) degrees of freedom. The energy spectrum in presence of the magnetic field is given as

$$\epsilon = \pm \sqrt{\left[\frac{\hbar^2 k_{\perp}^2}{2m^*} - m_0 \right]^2 + v^2 \hbar^2 k'_z^2} \pm b. \quad (3)$$

Note that even in presence of the Zeeman term, the extremal orbits occur at $k'_z = 0$.

On applying a magnetic field $\mathbf{B} = (0, 0, B)$ perpendicular to the nodal loop, the modified Hamiltonian can be obtained with vector potential \mathbf{A} expressed in the Landau gauge as $\mathbf{A} = (-By, 0, 0)$. One can rewrite the Hamiltonian as

$$H(B) = H_0 + \frac{e\hbar}{m} \left(-k_x B y + \frac{eB^2 y^2}{2\hbar} \right) \sigma_z \tau_0 + b \sigma_0 \tau_z \quad (4)$$

which, in the basis of Landau states^{10,13,14}, is written as

$$H(B) = \left[\left(n + \frac{1}{2} \right) \frac{e\hbar B}{m^*} - m_0 \right] \sigma_z \tau_0 + v \hbar k_z \sigma_y \tau_0 + b \sigma_0 \tau_z. \quad (5)$$

So the dispersions take the form

$$\epsilon_{n,k_z} = \pm \sqrt{\left[\left(n + \frac{1}{2} \right) \frac{e\hbar B}{m^*} - m_0 \right]^2 + v^2 \hbar^2 k_z^2} \pm b. \quad (6)$$

Since k_z is not affected by \mathbf{B} , the 3D problem decomposes into a family of 2D ones parametrized by k_z ¹⁵. And for each k_z , we find discrete Landau level states (given by index n) with huge degeneracy that is also proportional to the magnetic field strength B .

III. QUANTUM OSCILLATIONS

As a magnetic field variation causes Landau tubes to change their widths as well as allow them to successively cross through the Fermi surface (FS), the Fermi energy (or chemical potential μ) or magnetization M_z quite naturally show fluctuations with such field variations. For now, here we start with $m^* = m$, the free electronic mass.

One can calculate the magnetization or total number of particles/electrons N from the free energy and thermodynamic potentials as $F = E - TS$ and $\Omega = F - \mu N$ respectively. In this paper we present a zero temperature analysis where one can obtain

$$\delta\Omega = D \sum_{\epsilon_n \leq \mu} (\epsilon_n - \mu) \quad (7)$$

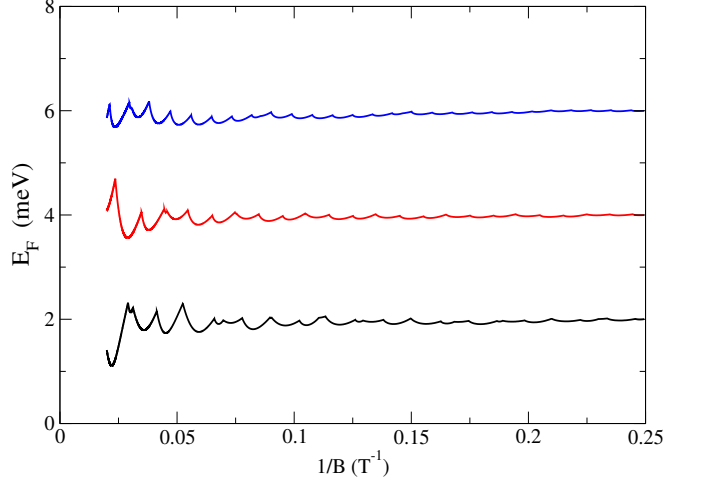


FIG. 1: Fluctuation in Fermi level plotted against inverse of field strength B^{-1} for three different N values.

with the sum over Landau level index is restricted as shown. Here D is the degeneracy factor and is given by $D = \delta k_z \frac{qBV}{2\pi^2 \hbar^2}$, V being the volume of the sample. From Ω one can obtain M_z and N as $M_z = -\left(\frac{\partial\Omega}{\partial B}\right)_\mu$ and $N = -\left(\frac{\partial\Omega}{\partial\mu}\right)_B$. If we disregard the Zeeman term (just for ease of calculation to start with) and integrate Eq.7, one can obtain the thermodynamic potential as

$$\Omega = \frac{qBV}{2\pi^2 \hbar^2 v} \sum_n \left\{ \frac{x_n^2}{2} \log \left| \frac{\mu + y_n}{\mu - y_n} \right| - \mu y_n \right\}. \quad (8)$$

The sum includes those integers n for which $y_n^2 = \mu^2 - [(n + 1/2)\mu_B B - m_0]^2 = \mu^2 - x_n^2 \geq 0$. From there one gets the expression for N as

$$N = \frac{qBV}{\pi^2 \hbar^2 v} \sum_{|\mu| > |x_n|} \sqrt{\mu^2 - [(n + 1/2)\mu_B B - m_0]^2}. \quad (9)$$

Considering constancy of N with field variation, one can numerically obtain the variation of Fermi energy E_F (or μ) with B as shown in Fig.1. There are quite a few things that this plot indicates. First of all, quantum oscillation dominates at large B values. The oscillation shows a constant periodicity when plotted against inverse of field. Thirdly, we notice huge fluctuations at very large B values because very few Landau tubes can remain within the Fermi surface chosen here.

Next we consider M_z , the magnetization parallel to field direction. We switch on the Zeeman term and with that the M_z expression becomes

$$\begin{aligned} M_z = & \frac{qV}{2\pi^2 \hbar^2 v} \left[\sum_{|\mu_+| > |x_n|} \left\{ \mu_+ y_n - x_n \left(\frac{3x_n}{2} + m_0 \right) \ln \frac{\mu_+ + y_n}{\mu_+ - y_n} \right. \right. \\ & \left. \left. + 2by_n \right\} + \sum_{|\mu_-| > |x_m|} \left\{ \mu_- y_m - \right. \right. \\ & \left. \left. x_m \left(\frac{3x_m}{2} + m_0 \right) \ln \frac{\mu_- + y_m}{\mu_- - y_m} - 2by_m \right\} \right] \end{aligned} \quad (10)$$

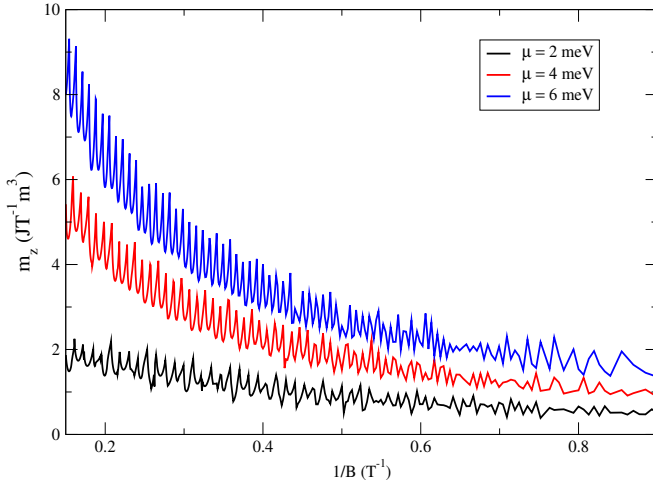


FIG. 2: Variation of M_z with inverse of field strength B^{-1} for different(average) μ values.

where $\mu_{\pm} = \mu \pm b$ and

$$\frac{x_n}{x_m} = \frac{(n + \frac{1}{2})\mu_B B - m_0}{(m + \frac{1}{2})\mu_B B - m_0}, \quad \frac{y_n}{y_m} = \frac{\sqrt{\mu_{+}^2 - x_n^2}}{\sqrt{\mu_{-}^2 - x_m^2}}.$$

Typical plots for m_z ($m_z = M_z/V$) variation with $1/B$ is shown in Fig.2. It shows the quantum oscillations in the data for m_z whose amplitude increases with the strength of B . One can analytically understand such variations as sum of sinusoidal oscillations which we discuss in the next section.

IV. EFFECTIVE MASS VARIATION AND ZEEMAN CONTRIBUTION

Quantum oscillation measurements of Shubnikov de Haas or De-Haas Van Alphen experiments in NLSM systems like $ZrSiS$ ¹⁶, $CaAgAs$ ¹⁷ or Dirac material $PtBi_2$ ¹⁸ show signatures of light effective masses and high quantum mobilities in electronic carriers. They exhibit two oscillations frequencies coming from α and β pockets in the Fermi surfaces. Our model Hamiltonian also indicates two extremal area of cross-sections in the low energy FS (though the number of QO frequencies doubles on considering the Zeeman term). The oscillating magnetization data, when subtracted from the smooth paramagnetic background can be analyzed using Fast Fourier transformation (FFT) and thereby the oscillation frequencies are estimated in experiments. Theoretically such behavior can be described using a Lifshitz-Koservich (LK) formula. It shows ΔM , the fluctuation in magnetization (such that $\Delta M = M - M_{\text{average}}$) as sum of oscillating functions each corresponding to a QO frequency F as

$$\Delta M \propto -B^{1/2} R_T R_D R_S \sin[2\pi(\frac{F}{B} - \gamma - \delta)]. \quad (11)$$

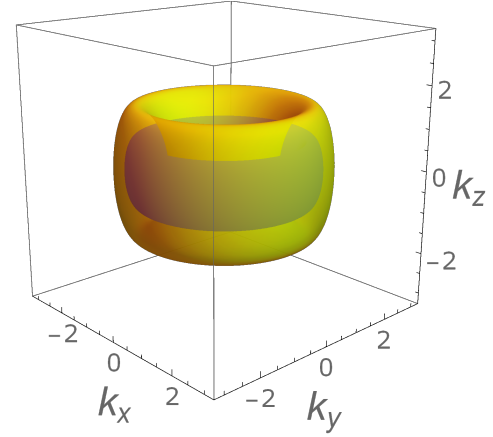


FIG. 3: Typical Fermi surfaces in presence of the Zeeman term. Generally two distinct surfaces (for \uparrow and \downarrow electrons respectively) give 4 extremal surfaces and hence 4 QO frequencies.

This depends on the effective mass m^* through the thermal damping factor $R_T = (\alpha T m_r / B) / \sinh(\alpha T m_r / B)$, $R_D = \exp(-\alpha T_D m_r / B)$ and $R_S = \cos(\pi g m_r / 2)$ where $\alpha = 2\pi^2 k_B m / (\hbar c)$, $m_r = m^* / m$ and T_D is called the Dingle temperature¹⁶⁻¹⁸. Besides, the first phase term $\gamma = 1/2 - \phi_B / 2\pi$ with ϕ_B being the Berry phase and the second phase term $\delta = \pm 1/8$ in 3D¹⁶. Usually m^* is obtained via fitting the thermal damping factor R_T of the LK formula with the experimentally obtained variation of the FFT amplitudes with temperature. At zero temperature and considering infinite relaxation time for electrons, one can write, for multiple QO frequencies, $\Delta M = B^{1/2} \sum_i C_i(m_r) \sin[2\pi(\frac{F_i}{B} - \gamma_i - \delta_i)]$, where the prefactors C_i depend on m_r . In our calculations later, we artificially vary m^* to see its effects on the spectral results as well.

Now let us get estimates/expressions of these QO frequencies for our NLSM system. Without the Zeeman term, the toroidal Fermi surface gives two extremal surfaces for nonzero μ (with $\mu < m_0$) values in the $k_z = 0$ plane with magnetic field along the z direction. These will be given by

$$A_{ex}^{\pm} = \frac{2\pi m^*}{\hbar^2} (m_0 \pm \mu) \quad (12)$$

and following Onsager's relation it leads to two fundamental QO frequencies $F^{\pm} = \frac{\hbar}{2\pi e} A_{ex}^{\pm} = \frac{m^*}{\hbar e} (m_0 \pm \mu)$. But as we turn on the Zeeman term, one gets two toroidal Fermi surfaces (see Fig.3) at low energies and we need to consider two pairs of fundamental frequencies which can be designated as

$$F_{\uparrow}^{\pm} = \frac{m^*}{\hbar e} (m_0 \pm (\mu + b)) \quad \& \quad F_{\downarrow}^{\pm} = \frac{m^*}{\hbar e} (m_0 \pm (\mu - b)) \quad (13)$$

respectively. This is however valid as long as $m_0 > \mu + b$ and b small. For $b < \mu$ and $m_0 < \mu + b$, there will be

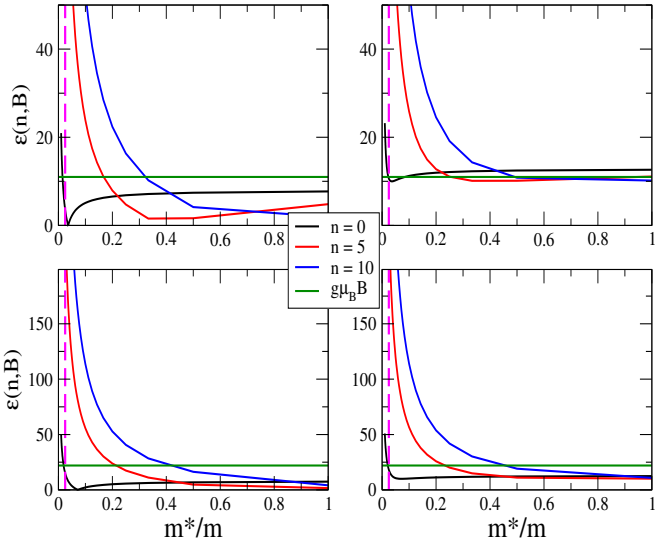


FIG. 4: (Color online) Energy spectrum for $vp_z = 0$ (left) and $vp_z = 10$ meV (right) as well as for $B = 5T$ (top) and $B = 10T$ (bottom) respectively. The Zeeman term with $g = 38$ is included and the value of $m_r = 0.025$ is highlighted (magenta dashed line) as well.

3 QO frequencies. But for $b > \mu$, we need to consider 2 (for $m_0 > \mu + b$) or 1 (for $m_0 < \mu + b$) QO frequencies. Notice that the Zeeman term causes the frequencies to vary linearly with magnetic field B now. So periodicity with B^{-1} gets lost which is noticeable particularly when b is large.

The quantum oscillation in these systems feature strong Zeeman splitting at high fields and at low temperatures. This can be realized from Eq.13 as well (compare F_{\uparrow}^+ , F_{\downarrow}^+ pair or F_{\uparrow}^- , F_{\downarrow}^- pair). As QO amplitudes increases with field magnitude, the Zeeman splitting of QO peaks (as seen from the FFT spectra) is easily discernible for large magnetic fields. Now we should remember that the Lande g factor for an electron in a band gets modified from its free electron value of $g = 2$ due to spin-orbit couplings. In the present problem, this gets enlarged to very high values depending on the effective mass m^* (see Ref.19) and proportional to the Zeeman splitting of the LL spectra. Experimentally this is calculated as $\frac{g}{2} \frac{m^*}{m} = F(\frac{1}{B^+} - \frac{1}{B^-})$ where B^{\pm} denote two fields at the position of the split peaks in the magnetization plot.

Here we will use $g = 38$ and $m^* = 0.025m$, following the findings for NLSM compound $ZrSiS^{16}$ in order to analyze the effect of Zeeman effect on the NLSM spectra. From Eq.6, we find that the spectra varies with m^* and it will be interesting to compare such variation with the Zeeman splitting (which is $2b$) to determine the importance of the latter. In Fig.4, we show such variations which indicate huge m^* dependence on LL dispersions. We find that the Zeeman contribution remains significant in the free electron limit with $m^* = m$, but becomes insignificant in the massless limit $m^* \rightarrow 0$. For small masses like $m_r = 0.025$, as observed in $ZrSiS^{16}$,

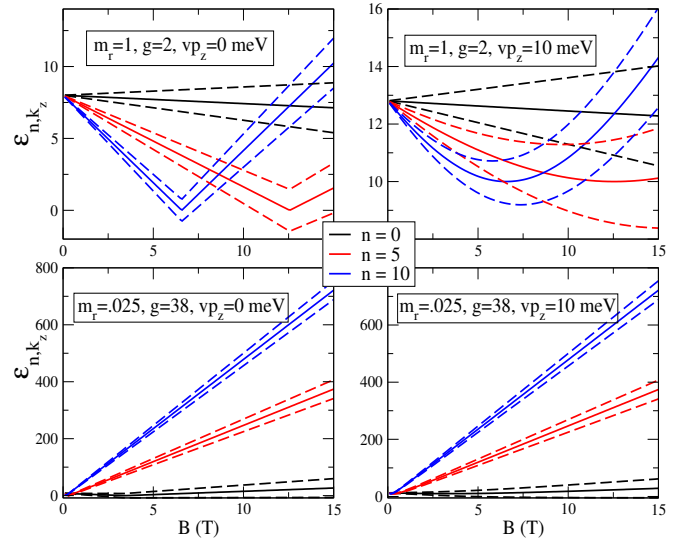


FIG. 5: Variation of energy spectrum for $vp_z = 0$ (left) and $vp_z = 10$ meV (right) with magnetic field B both with (dashed lines) and without (solid lines) the Zeeman term.

Zeeman term remains significant only for a few LL such as $n = 0$ (see Fig.4). The Zeeman term becomes important whenever the energy gap is reduced considerably (*i.e.*, $gap \leq 2b$). It depends not only on m^* but also on n values. Notice that for the other modes with $n = 5, 10$, the Zeeman contribution is negligible for very small m^* values. For $p_z \neq 0$ the Zeeman term becomes even less important as the lower cut-off of energy magnitude becomes nonzero as well. One can also see such behavior from field dependence of the LL spectra as shown in Fig.5 where the smallness of Zeeman contribution is clearly seen for the small effective mass of $m^* = 0.025m$ (even after an enlarged $g = 38$ is considered).

The situation differs for different kind of systems. For example, in GaAs-based heterostructures¹⁴, the effective mass is taken to be $m^* \sim 0.07m_e$ which increases the cyclotron frequency almost tenfold. On the other hand, Zeeman term also get reduced with $g \sim 0.44$. So Zeeman splitting is very small fraction of the LL spacings and its contribution can be neglected. However for NLSM systems, *e.g.*, in the compound $ZrSiS$, the combination of effective mass reduction and lande-g factor increase causes the Zeeman splitting to often become comparable to the LL energy spacings.

V. DENSITY OF STATES

Unlike the 3D free electron gas where the Hamiltonian can be decoupled to two independent motions along and perpendicular to the field direction, our present problem constitutes a two level system where the dispersion, *i.e.*, Eq.6, is not just sum of contributions from motions parallel and perpendicular to field directions. Thus energy convolution²⁰ can not be utilized to obtain the density of

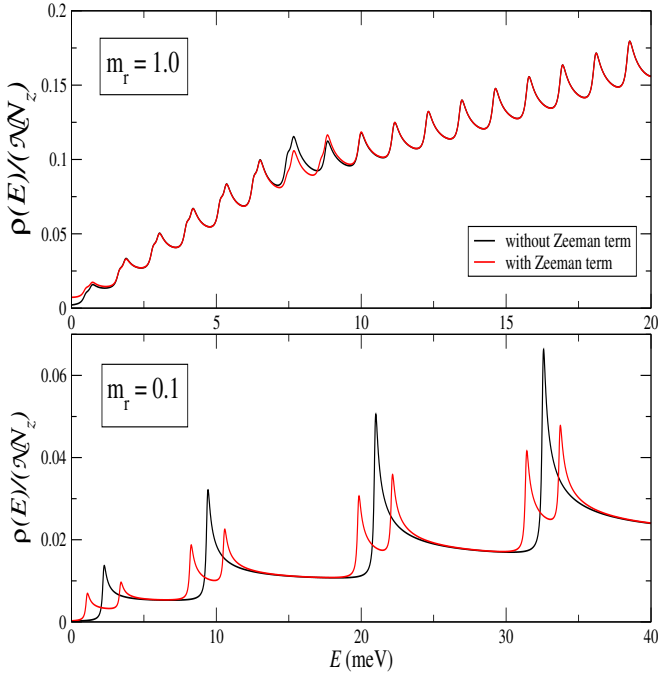


FIG. 6: DOS plots for $B = 10T$ and $m_0 = 8\text{meV}$ with both with and without the Zeeman term included for $m_r = 1$ (top) and $m_r = 0.1$ (bottom). $g = 2$ is considered for both the plots.

states (DOS). Rather it is obtained from the basic definition as

$$\rho(E) = \mathcal{N} \sum_{n,k_z} \delta(E - \epsilon_{n,k_z}) \quad (14)$$

where $\mathcal{N} = eBA/h$ denotes the degeneracy factor, A being the area of the sample in the xy plane (*i.e.*, plane normal to the field direction). Numerically one can obtain $\rho(E)$ using Lorentzian approximation of the delta function as

$$\delta(E - \epsilon_{n,k_z}) = Lt_{\eta \rightarrow 0} \frac{1}{\pi} \frac{\eta}{(E - \epsilon_{n,k_z})^2 + \eta^2}. \quad (15)$$

Furthermore, a sum for Landau levels upto $n = 100$ is considered and using periodic boundary conditions we take $k_z = \frac{2\pi}{N_z a_0} \nu$ where N_z denotes the total number of k_z points along z direction, ν is a non-negative integer with $\nu \leq N_z$ and a_0 is the separation between successive k points along z . In Fig.6, we show the DOS plots for $m^* = m$ and $m^* = m/10$ respectively for $B = 10T$ and $m_0 = 8 \text{ meV}$. Notice that the peak positions in DOS almost retains their peak positions as the Zeeman term is turned on for $m_r = 1$. This is because the Zeeman splittings become same as the Landau level spacings. On the other hand, for a smaller $m_r = 0.1$ one can see the differences in peak positions between DOS plots with and without the Zeeman term as the LL spacings becomes much wider compared to the Zeeman splitting.

VI. FIELD PARALLEL TO THE NODAL PLANE

Magnetic oscillations at low energies become topological when the magnetic field directs parallel to the nodal plane and hence this is important in its own right. The Hamiltonian for the NLSM in presence of field parallel to \hat{x} direction can be given as

$$H = \left(\frac{\hbar^2 k_\perp^2}{2m^*} - m_0 \right) \sigma^z \tau^0 + vp_z \sigma^y \tau^0 + b \sigma^0 \tau^x. \quad (16)$$

We consider the Magnetic field to be $\mathbf{B} = (B, 0, 0)$ and the vector potential $A = (0, -Bz, 0)$. The Hamiltonian gets modified via Peierls substitution $\mathbf{p}' = \mathbf{p} - \mathbf{eA}$, to become:

$$H = \left[\frac{p_x^2}{2m} + \frac{(p_y + eBz)^2}{2m} - m_0 \right] \sigma^z \tau^0 + vp_z \sigma^y \tau^0 + b \sigma^0 \tau^x \quad (17)$$

Now, we introduce the variable,

$$\tilde{z} = (z + \frac{p_y}{eB}) \quad (18)$$

that transforms Eq.17 as

$$H = \left[\frac{m\omega_c^2 \tilde{z}^2}{2} - m'_0 \right] \sigma^z \tau^0 + vp_z \sigma^y \tau^0 + b \sigma^0 \tau^x \quad (19)$$

where $m'_0 = m_0 - \frac{p_y^2}{2m}$. This Hamiltonian can be numerically diagonalized to get the energy eigenvalues and one can obtain various quantities like density of states from there.

One can get a dimensionless form of the Hamiltonian by defining parameters¹⁰ $\delta = (\frac{2m'^3}{m\hbar^2 \omega_c^2 v^2})^{\frac{1}{3}}$, $\alpha = (\frac{2v}{m\omega_c^2 \sqrt{\hbar}})^{\frac{1}{3}}$, $Z = \frac{\tilde{z}}{\alpha \sqrt{\hbar}}$, $P = \frac{\alpha p_z}{\sqrt{\hbar}}$, and $C = \frac{2b}{\alpha^2 m \omega_c^2 \hbar}$. This results in the following restructuring of the Hamiltonian:

$$H = \left[\frac{m\hbar^2 \omega_c^2 v^2}{2} \right]^{\frac{1}{3}} [(Z^2 - \delta) \sigma^z \tau^0 + P \sigma^y \tau^0 + C \sigma^0 \tau^x] \quad (20)$$

which gives the eigenvalues as

$$E = \left(\frac{m\hbar^2 \omega_c^2 v^2}{2} \right)^{\frac{1}{3}} [\pm \sqrt{(Z^2 - \delta)^2 + P^2} \pm C] \quad (21)$$

Typical positive spectra for $p_x = 0$ (where Landau tubes can cross the Fermi surfaces extremely) are shown in Fig.7 in presence/absence of the Zeeman term. Unlike the case with $\mathbf{B} = B\hat{z}$, here the Zeeman splitting does not put enough impact as the dispersion energy levels in the present case are comparatively more spread out. Notice that the topological regime, which occurs before the splitting of the degenerate bands at low energies $E \sim m_0$, become narrower for smaller effective masses. Thus non-trivial oscillations can be observed only for small values of B alone, whenever the NLSM compounds possess small m^* values for the band electrons.

Next we probe the DOS only at low energies. The DOS indicates occupation at zero energies. In fact that

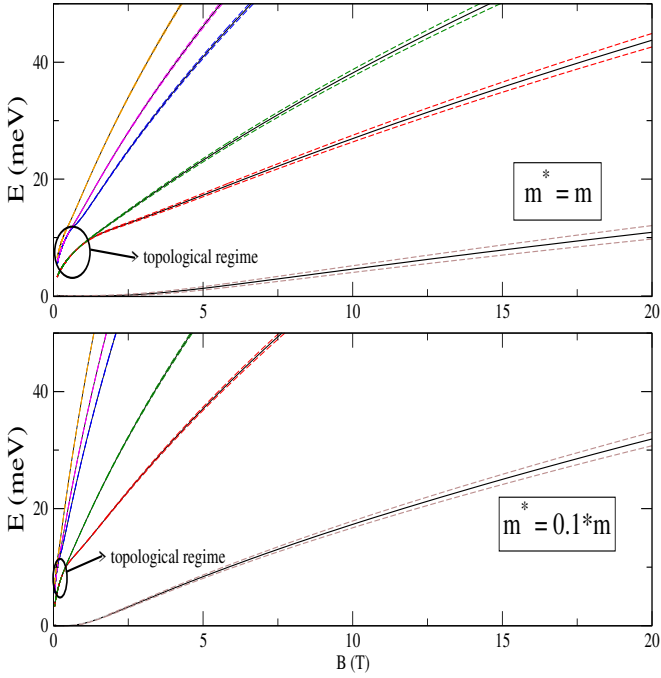


FIG. 7: Dispersions in the $p_x = 0$ plane in presence (dashed lines) /absence (solid lines) of Zeeman term with effective mass $m^* = m$ (top) and $m^* = 0.1 * m$ (bottom).

is the most prominent peak in the DOS. At low energies, one can find few other discrete peaks though they don't appear with fixed periodicity what one would get corresponding to the multiple of cyclotron frequencies if the field acts perpendicular to nodal plane (*i.e.*, $\mathbf{B} = B\hat{z}$). This is because for $\mathbf{B} = B\hat{x}$, the electron motion is all coupled among the three spatial directions. One can at most say that for motion perpendicular to the field direction, *i.e.*, for motion in the yz plane, the low energy spectra can be written as $E_n(p_x) = f(p_x)\sqrt{n}$, $f(p_x)$ being some function of p_x and n a positive integer. Moreover, as we consider a smaller m^* instead, a number of characteristic changes occur in the DOS. Most of the weights shift to higher energies. The zero energy peak moves to higher values with much reduced probability of occupation. One gets a series of low intensity low energy peaks, similar to that are seen for $m^* = m$ as well and major peaks are obtained only for $E > m_0$. These are again the outcome of spreading out of the spectra due to smaller m^* values in compatible with Eq.21. With Zeeman coupling, all the peaks are bifurcated and these can be seen in the DOS plots of the Fig.8.

VII. SUMMARY

In this paper, we have gone a long way to describe what happens in a simple type I NLSM model as a magnetic field is applied on it and its magnitude is varied through. We quantify the the fluctuation in the Fermi

level with the variation in the field strength which increases for larger field values. Then we calculate the quantum oscillation in parallel magnetization and its periodicity as well as decay with $1/B$. The effect of effective mass reduction and Zeeman splitting is vividly described both for field perpendicular to the nodal plane as well as for field parallel to it. Topological oscillations are reported in the latter case for small energies^{8–10}. We find such topological regime to become narrower as the effective mass is reduced. The DOS features are examined and the preference of occupation for the electrons are mentioned and discussed.

Our work can give useful guide on what to expect from the LL spectra, DOS and quantum oscillations in presence of Zeeman splitting, reduced effective masses and enlarged Lande-g factors. Moreover, the Fermi surface structures and QO frequencies can help understanding the FFT spectra obtained from NLSM compounds during quantum oscillations. As a continuation of the present work, one can also study the inter LL transfers of electrons or the defect productions²¹ once periodic variation of the magnetic field¹⁰ is considered in presence of Zeeman coupling and reduced m^* values. And it will be equally interesting to probe the entanglement generation²² in NLSM systems following the Floquet Hamiltonian²³ corresponding to such periodic driving involving an oscillating magnetic field.

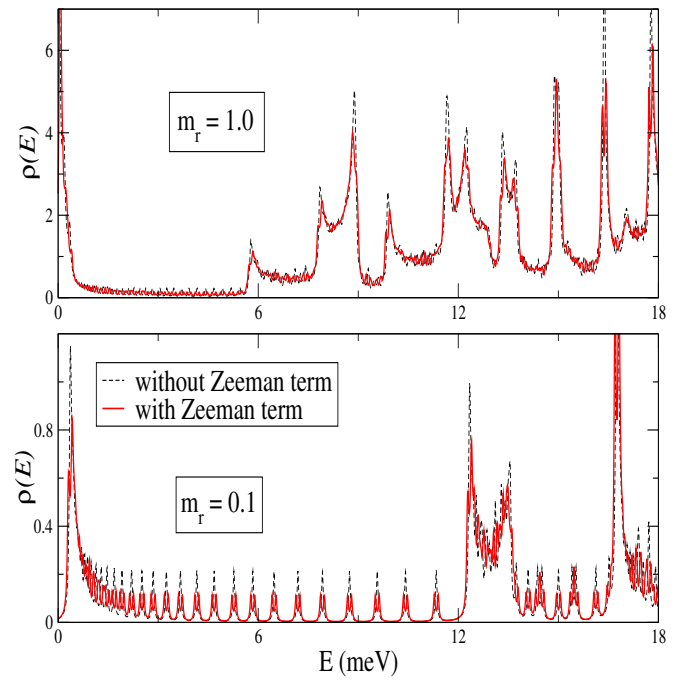


FIG. 8: Low energy DOS plots for $B = 1T$ and $m_0 = 12meV$ with both with and without the Zeeman term included for $m_r = 1$ (top) and $m_r = 0.1$ (bottom). Here $g = 2$ is considered for both the plots.

Acknowledgements

This work is financially supported by DST-SERB, Government of India under grant no. SRG/2019/002143.

¹ T. T. Heikkil, G. E. Volovik, JETP Lett. **93**, 59 (2011); A. A. Burkov *et al.*, Phys. Rev. B **84**, 235126 (2011).

² C. Fang *et al.*, Phys. Rev. B **92**, 081201(R) (2015).

³ C. Fang *et al.*, Chin. Phys. B, Vol.**25**, No. 11, 117106 (2016).

⁴ A. Bernevig *et. al.*, Jour. Phys. Soc. Jpn.**87**,041001 (2018).

⁵ S. Q. Shen, “Topological Weyl and Dirac Semimetals”, Springer publication (2017).

⁶ N. P. Armitage *et al.*, Rev. Mod. Phys.**90**, 015001 (2018).

⁷ S.Kar, A. Jayannavar, Asian Jour. Res. and Rev. in Phys. **4**(1) 34-45 (2021).

⁸ H. Yang, R. Moessner and L.-K. Lim, Phys. Rev. B**97**, 165118 (2018).

⁹ L. Oroszlany *et al.*, Phys. Rev. B**97**, 205107 (2018).

¹⁰ S.kar, Jour. Phys. Cond. Mat. **33**, 225601 (2021).

¹¹ C. Li *et al.*, Phys. Rev. Lett.**120**, 146602 (2018).

¹² K. Taguchi *et al.*, Phys. Rev. B**94**, 155206 (2016).

¹³ R. A. Molina, and J. Gonzalez, Phys. Rev. Lett**120**, 146601 (2018).

¹⁴ P.Fazekas, “Lecture Notes on Electron Correlation and Magnetism” World Scientific Publishing (2003).

¹⁵ L.-K. Lim, and R. Moessner, Phys. Rev. Lett**118**, 016401 (2017).

¹⁶ J. Hu *et al.*, Phys. Rev. B**96**, 045127 (2017).

¹⁷ Y. H. Kwan *et.al.*, Phys. Rev. Res.**2**, 012055(R) (2020).

¹⁸ W. Gao *et al.*, Science Bulletin **64**, 1496 (2019).

¹⁹ G. W. Winkler *et al.*, Phys. Rev. Lett.**119**, 037701 (2017).

²⁰ L. H. Bennett, “Electronic Density of States”, U.S. National Bureau of Standards (1971).

²¹ S. N. Shevchenko *et al.* , Phys. Rep. 492, 1 (2010); S. Kar *et. al.*, Phys. Rev. B **94**, 075130 (2016); S. Kar, Phys. Rev. B **95**, 085147 (2017).

²² S. Kar *et. al.*, Phys. Rev. B **98**, 245119 (2018).

²³ A. Eckart, and E. Anisimovos, New J. Phys. **17**, 093039 (2015).